Analysis of the Sideband Electromagnetic Noise in Permanent Magnet Synchronous Motors Generated by Rotor Position Error

Wenzhe Deng, *Member*, *IEEE*, and Shuguang Zuo

***Abstract*—The influence of rotor position error generated by resolver on electromagnetic noise of permanent magnet synchronous motors (PMSMs) is analyzed in this paper. The motor noise is mainly caused by the electromagnetic force acting on the surface of stator teeth or permanent magnets. Firstly, the influence of rotor position error on current harmonics is deduced theoretically. The spatial and temporal characteristics of the electromagnetic force are then analyzed. The results show that the rotor position error will introduce extra sideband frequency harmonics to the current and electromagnetic force. This will lead to more abundant noise harmonics. The field-oriented control (FOC) model and the electromagnetic finite element model (FEM) are then established to simulate the influence of rotor position error on current harmonics and electromagnetic force. Finally, a test is carried out to capture the phase current and noise spectrum. Both the simulation and test results are consistent with the theoretical analysis results. This study can give a reference to the source identification and optimization of acoustic performance for PMSMs in electric vehicles.**

***Index Terms*— PMSM, electromagnetic force, rotor position error, sideband harmonic, noise.**

I. INTRODUCTION

Permanent magnet synchronous motors (PMSMs) have been widely used in electric vehicles due to their high efficiency, high power density, and wide speed range [1]. The driven motors replace traditional internal combustion engines in electric vehicles and serve as the power assembly. This leads to the motors one of the main sources of acoustic noise for electric vehicles. The sound pressure level of electric motors is relatively lower than that of internal combustion engines. However, its frequency is higher and distributed in the sensitive frequency band of the human ear, which leads to poor subjective feeling. The study of electromagnetic noise of PMSMs is of great significance for the improvement of vibroacoustic quality and comfort for electric vehicles.

The electromagnetic forces acting on the surface of stator teeth and permanent magnets (PMs) cause the motor structure to vibrate and radiate acoustic noise furtherly. Several research works have engaged in the electromagnetic vibration and noise of the electric motors, mainly focused on the prediction model [2-4], mechanism analysis [5-7], and reduction method [8-10] of electromagnetic noise, etc. The space vector pulse width modulation (SVPWM) method is getting more usage in industrial applications to drive the PMSMs. In addition to the fundamental component, the phase current under ideal conditions contains $(6k\pm1)$th current harmonics and high-frequency current harmonics around the switching frequency as well. Here, k is an integer. The characteristics of electromagnetic noise considering the current harmonics of electric motors have drawn extensive attention and research [11, 12]. However, the current waveform under actual working conditions is not generally ideal. More orders or even fractional-order current harmonics can be found in the phase current spectrum [13, 14]. This leads to new features of the electromagnetic noise characteristics in electric motors, and brings barriers to the source identification of acoustic noise for electric motors.

With the advantage of simple structure and well robustness, the resolvers have been widely used in the PMSMs for vehicle applications to capture the position angle of the rotor [15, 16]. Due to the poor working conditions of the vehicle, certain errors will exist in the position signals output by the resolver decoding circuit inevitably. As the PMSM is driven by the field-oriented control (FOC) technique, the transformation from d-q to three-phase stator coordinate will bring extra frequency components to the phase current further. Currently, the rotor position error and its effect on current harmonics have drawn extensive attention and research. In [17], the effect of non-ideal factors on the output angle of the resolver is analyzed, and a corresponding compensation method is proposed. It is found in [18] the tested noise spectrum contains extra sideband harmonics, but the influence of the rotor position error on the whole frequency band current harmonics and electromagnetic noise is not further analyzed. In [19], the effect of rotor position error on the torque ripple and longitudinal vibration of electric wheel system are investigated based on a dynamic model. The position error will enlarge the resonance frequency band. This greatly worsens the longitudinal vibration of the electric wheel system. Current studies only focus on the influence of the rotor

This work was supported by the National Natural Science Foundation of China under Grant 51875410.

Wenzhe Deng is with the School of Electrical Engineering and Automation, Anhui University, Hefei 230601, China, and the National Engineering Laboratory of Energy-Saving Motor and Control Technology, Anhui University, Hefei 230601, China (e-mail: deng_wenzhe@foxmail.com).

Shuguang Zuo is with the School of Automotive Studies, Tongji University, Shanghai 201804, China (e-mail: sgzuo@tongji.edu.cn).

position error on the fundamental current or low-frequency current harmonics, without considering the high-frequency harmonic around the switching frequency. Since the rotor position error introduce extra sideband current harmonics, the temporal and spatial distribution of the electromagnetic force will be affected furtherly. This will result in new features of the electromagnetic vibration and noise characteristics of PMSMs consequently. However, there are few studies focusing on the influence of the rotor position error on the motor vibration and noise so far. Based on the state of the art, the novelty of this study lies in that it reveals the vibroacoustic mechanism of PMSMs generated by the rotor position error in full frequency band, through the analysis of effect of position error on current harmonics and electromagnetic force. This study can provide guidance for the source identification and optimization of acoustic noise for PMSMs in electric vehicles.

This paper is organized as follows. In Section II, the rotor position error is firstly derived analytically. The influence of position error on low-frequency and high-frequency current harmonics, electromagnetic force, and acoustic noise is analyzed. In Section III, the field-oriented control (FOC) model and the electromagnetic finite element model (FEM) are established to simulate the influence of rotor position error on current harmonics and electromagnetic force with and without position error. Finally, the theoretical analysis is verified by noise test in Section IV.

II. THEORETICAL ANALYSIS

A. General Description of the Resolver

The position sensor adopted in the driven motor is the resolver, which is a variable reluctance motor. The resolver contains two orthogonal windings and an excitation winding. When the excitation winding is input with a high-frequency AC signal, sine and cosine signals will be induced in the two orthogonal windings. The schematic diagram of the resolver is shown in Fig.1.

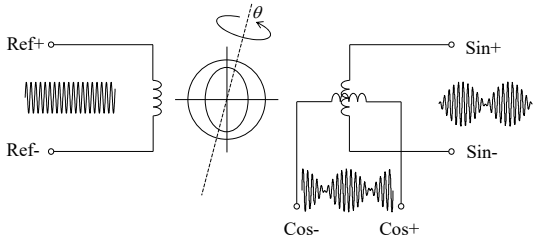

Fig. 1. Schematic diagram of the resolver

For the ideal resolver, the output signal U_{sin} and U_{cos} can be expressed as

$$\begin{aligned} U_{\sin} &= KE\sin\theta \\ U_{\cos} &= KE\cos\theta \end{aligned} \tag{1}$$

where, KE is the excitation level of the resolver, θ is the electric angle of the resolver.

The error voltage is written as

$$\begin{aligned} U_{err} &= U_{\sin}\cos\varphi - U_{\cos}\sin\varphi \\ &= KE\sin(\theta\text{-}\varphi) \end{aligned} \tag{2}$$

where, φ is the output decoded angle of the resolver. The error voltage should be as small as possible, so that the output angle φ is closer to the actual angle θ.

When the error voltage is equal to zero, the output angle of the ideal resolver is calculated from

$$\varphi = \arctan\frac{U_{\sin}}{U_{\cos}}. \tag{3}$$

B. Rotor Position Error

The actual working conditions of driven motors for vehicle applications are relatively poor, especially for the in-wheel motors. This causes the output signal U_{sin} and U_{cos} is not ideal sine and cosine signals. It is accompanied by errors, like amplitude imbalance, imperfect quadrature, and dc offset, etc. These errors will lead to the distortion of the output rotor position angle.

The output signal U_{sin} and U_{cos} considering the non-ideal factors can be expressed as [18, 20]:

$$\begin{aligned} U_{\sin} &= KE\sin(\theta+\beta)+U_{offset} \\ U_{\cos} &= KE(1+\alpha)\cos\theta \end{aligned} \tag{4}$$

where, α, β and U_{offset} are the errors caused by amplitude imbalance, imperfect quadrature, and dc offset, respectively.

According to [20], the value of α, β and θ-φ is small, thus $\sin\beta\approx\beta$, $\cos\beta\approx1$ and $\sin(\theta\text{-}\varphi)\approx\theta\text{-}\varphi$. Substituting (4) into (2), the error voltage can be written as:

$$\begin{aligned} U_{err} &= \left[KE\sin(\theta+\beta)+U_{offset}\right]\cos\varphi - \left[KE(1+\alpha)\cos\theta\right]\sin\varphi \\ &= KE\begin{pmatrix}\sin\theta\cos\beta\cos\varphi+\sin\beta\cos\theta\cos\varphi \\ -\cos\theta\sin\varphi\text{-}\alpha\cos\theta\sin\varphi\end{pmatrix}+U_{offset}\cos\varphi \\ &\approx KE\left[\sin(\theta-\varphi)+\beta\cos\theta\cos\varphi-\alpha\cos\theta\sin\varphi\right] \\ &\quad +U_{offset}\cos\varphi. \end{aligned} \tag{5}$$

The decoding circuit forces the error voltage to zero, thus the rotor position error can be approximately expressed as:

$$\begin{aligned} \theta_{err} &= \theta-\varphi\approx\sin(\theta-\varphi) \\ &= \alpha\sin\varphi\cos\theta-\beta\cos\varphi\cos\theta-\frac{U_{offset}}{KE}\cos\varphi \\ &\approx \frac{\alpha}{2}\sin(2\theta)-\frac{\beta}{2}(1+\cos2\theta)-\frac{U_{offset}}{KE}\cos\theta. \end{aligned} \tag{6}$$

The relationship between the electric angel of the resolver and the PMSM is written as

$$P_r = \frac{p_{resolver}}{p} = \frac{\theta}{\theta_e} \tag{7}$$

where, $p_{resolver}$ and p are the pole pair number of the resolver and the PMSM, respectively.

Substituting (7) into (6), the rotor position error is calculated as:

$$\theta_{err} \approx \frac{\alpha}{2}\sin(2P_r\theta_e)-\frac{\beta}{2}(1+\cos2P_r\theta_e)-\frac{U_{offset}}{KE}\cos P_r\theta_e. \tag{8}$$

C. Effect of Rotor Position Error on Current Harmonics

According to the Clark and Park transformation, the relationship between the stator phase current and the dq-axis current is as follows,

$$\begin{pmatrix} i_a \\ i_b \\ i_c \end{pmatrix} = \begin{bmatrix} \cos\alpha_e & -\sin\alpha_e \\ \cos\left(\alpha_e - \frac{2\pi}{3}\right) & -\sin\left(\alpha_e - \frac{2\pi}{3}\right) \\ \cos\left(\alpha_e + \frac{2\pi}{3}\right) & -\sin\left(\alpha_e + \frac{2\pi}{3}\right) \end{bmatrix} \begin{pmatrix} i_d \\ i_q \end{pmatrix} \tag{9}$$

here,

$$\alpha_e = \theta_e - \theta_{err}. \tag{10}$$

The d-q axis current is assumed to be ideal as it is determined by the target torque. The rotor position error will affect the transformation matrix as the electric angle used is the output angle of the resolver. Next, the influence of the rotor position error on the phase current will be analyzed.

Besides the fundamental component, there are also low-frequency and high-frequency current harmonics near the switching frequency in the output current for the ideal inverter. Since the switching frequency of the electric motors for vehicle applications is high, usually up to 10000 Hz, the high frequency noise around twice or more of the switching frequency exceeds the sensitive range of the human ear. Hence, this paper will only focus on the main current harmonics around the first switching frequency. The ideal current in the q-axis can be expressed as,

$$\begin{aligned} i_q \approx\ & I_{q1} + I_{q\_6k}\left[\cos\left(6k\omega_1 t + \varphi_q\right)\right] \\ & + I_{q\_\omega_s \pm 3\omega_1}\left[\cos\left(\omega_s t \pm 3\omega_1 t + \varphi_q\right)\right]. \end{aligned} \tag{11}$$

Among which, the first item is the fundamental current, the second item is the low-frequency harmonics, the third item is the high-frequency current harmonics generated by the switching action of the inverter. The computation of the amplitude of low- and high-frequency current harmonics can refer to [21] and [22]. Here, ω_s is the switching angular frequency, ω_1 is the fundamental electrical angular frequency.

i_d=0 method is usually adopted for the surface-mounted PMSM. According to (9), A phase current can be written as,

$$\begin{aligned} i_a &= -i_q \sin\alpha_e \\ &= -i_q \sin\left(\theta_e - \theta_{err}\right) \\ &= i_q \cos\theta_e \sin\theta_{err} - i_q \sin\theta_e \cos\theta_{err}. \end{aligned} \tag{12}$$

Without position error, A phase current can be calculated from,

$$\begin{aligned} i_a &= -i_q \sin\theta_e \\ &= -\begin{Bmatrix} I_{q1} + I_{q\_6k}\left[\cos\left(6k\omega_1 t + \varphi_q\right)\right] \\ + I_{q\_\omega_s \pm 3\omega_1}\left[\cos\left(\omega_s t \pm 3\omega_1 t + \varphi_q\right)\right] \end{Bmatrix} \sin\theta_e \\ &= -\begin{Bmatrix} I_{q1}\sin\omega_1 t + \frac{1}{2} I_{q\_6k\pm1}\left\{\sin\left[(6k+1)\omega_1 t + \varphi_q\right] - \sin\left[(6k-1)\omega_1 t + \varphi_q\right]\right\} \\ + \frac{1}{2} I_{q\_\omega_s \pm 2\omega_1}\left[\sin\left(\omega_s t - 2\omega_1 t + \varphi_q\right) - \sin\left(\omega_s t + 2\omega_1 t + \varphi_q\right)\right] \\ + \frac{1}{2} I_{q\_\omega_s \pm 4\omega_1}\left[\sin\left(\omega_s t + 4\omega_1 t + \varphi_q\right) - \sin\left(\omega_s t - 4\omega_1 t + \varphi_q\right)\right] \end{Bmatrix}. \end{aligned} \tag{13}$$

If there exists position error, as the value of θ_{err} is small, $\sin\theta_{err} \approx \theta_{err}$, $\cos\theta_{err} \approx 1$. Equation (12) can be simplified as

$$i_a \approx i_q \theta_{err} \cos\theta_e - i_q \sin\theta_e. \tag{14}$$

Substituting (8) and (11) into (14), A phase current can be calculated from,

$$\begin{aligned} i_a = & -\begin{Bmatrix} I_{q1} + I_{q\_6k}\left[\cos\left(6k\omega_1 t + \varphi_q\right)\right] \\ + I_{q\_\omega_s \pm 3\omega_1}\left[\cos\left(\omega_s t \pm 3\omega_1 t + \varphi_q\right)\right] \end{Bmatrix} \sin\theta_e \\ & + \begin{Bmatrix} I_{q1} + I_{q\_6k}\left[\cos\left(6k\omega_1 t + \varphi_q\right)\right] \\ + I_{q\_\omega_s \pm 3\omega_1}\left[\cos\left(\omega_s t \pm 3\omega_1 t + \varphi_q\right)\right] \end{Bmatrix} \begin{Bmatrix} \frac{\alpha}{4}\left[\sin\left(1+2P_r\right)\theta_e - \sin\left(1-2P_r\right)\theta_e\right] \\ -\frac{\beta}{4}\left[\cos\left(1+2P_r\right)\theta_e + \cos\left(1-2P_r\right)\theta_e\right] - \frac{\beta}{2}\cos\theta_e \\ -\frac{U_{offset}}{2KE}\left[\cos\left(1+P_r\right)\theta_e + \cos\left(1-P_r\right)\theta_e\right] \end{Bmatrix}. \end{aligned} \tag{15}$$

The detailed derivation is given in the appendix. It can be seen from (15) that the left item is the phase current without position error, while the right item is the extra current harmonic brought by rotor position error.

According to the product to sum formula, (15) can be simplified as,

$$\begin{aligned} i_a = & I_{a1}^m \sin\left(1 \pm mP_r\right)\omega_1 t \\ & + I_{a\_6k\pm1}^m \left\{\sin\left[\left(6k \pm 1 \pm mP_r\right)\omega_1 t + \varphi_q\right]\right\} \\ & + I_{a\_\omega_s \pm 2\omega_1}^m \left[\sin\left(\omega_s t \pm 2\omega_1 t \pm mP_r\omega_1 t + \varphi_q\right)\right] \\ & + I_{a\_\omega_s \pm 4\omega_1}^m \left[\sin\left(\omega_s t \pm 4\omega_1 t \pm mP_r\omega_1 t + \varphi_q\right)\right] \end{aligned} \tag{16}$$

where m=0,1,2.

It can be seen from (13) and (16), there are only fundamental components, $(6k\pm1)$th and $(\omega_s \pm 2k\omega_1)$th harmonics in the phase current without the position error. While extra sideband harmonics with a frequency difference of $\pm 2P_r\omega_1$ and $\pm P_r\omega_1$ will be induced around the original current harmonics if the position error is introduced. The $\pm 2P_r\omega_1$ harmonics are generated by the amplitude imbalance and imperfect quadrature, and $\pm P_r\omega_1$ harmonics are generated by the dc offset error.

The three-phase currents only differ by 120 degrees in space, their frequency characteristics are the same. The frequency feature of the current harmonics with and without rotor position error is summarized in Table 1. Here, f_s is the switching frequency, f_1 is the fundamental electrical frequency.

TABLE I
FREQUENCY FEATURE OF CURRENT HARMONICS WITH AND WITHOUT ROTOR POSITION ERROR

	Without position error	With position error
Fundamental current	f_1	f_1 $f_1 \pm P_r f_1$ $f_1 \pm 2P_r f_1$
Low-frequency harmonics	$(6k\pm1)f_1$	$(6k\pm1)f_1$ $(6k\pm1)f_1 \pm P_r f_1$ $(6k\pm1)f_1 \pm 2P_r f_1$
High-frequency harmonics	$f_s \pm 2kf_1$	$f_s \pm 2kf_1$ $f_s \pm 2kf_1 \pm P_r f_1$ $f_s \pm 2kf_1 \pm 2P_r f_1$

D. Effect of Position Error on Electromagnetic Force

The vibration and noise of the electric motors are induced by the electromagnetic force acting on the surface of stator teeth or magnets. It can be seen from the previous section that the rotor position error mainly affects the phase current. This will change the armature reaction field furtherly. The PM field and the relative permeance are not relevant to the phase current, thus the position error has no influence on them.

The PMSM is fed by three-phase windings and the armature reaction field is the superposition of the magnetic fields generated by each phase winding. It can be calculated according to the arrangement scheme of the coil. The normal component of the magnetic field generated by a single coil can be expressed as [23]

$$b_z = N_c i \sum_{\nu=1}^{\infty} b_{z\nu} \cos \nu\theta. \tag{17}$$

The normal armature reaction field of A phase can be furtherly calculated from

$$B_{zA} = N i_a \sum_{\nu=1}^{\infty} b_{z\nu} k_{d\nu} \cos \nu\theta \tag{18}$$

where, N is the turn number of each phase. k_{dv} is the winding distribution factor, which depends on the arrangement scheme of the coil.

The superimposed magnetic field of three-phase can be simplified as

$$B_{z\_arm} = \sum_{\nu} B_{av}^{h} \sin\left(\nu N_t \theta + s_{v,h} \omega_h t\right) \tag{19}$$

where, N_t is the number of spatial periods of the PMSM. $s_{v,h}$ represents the rotation direction of the νN_tth armature reaction field. It is related to the pole-slot combinations and the current order. ω_h is the electrical angular frequency of hth current harmonic.

It can be seen from (19) when the position error is introduced, the frequency of the armature reaction field will also change due to extra frequency components of the current harmonics, but the spatial order remains unchanged.

The electric motor studied in this paper is an external-rotor in-wheel PMSM. The electromagnetic force acting on the surface of PMs is the main source of the vibration and noise for external-rotor motors. Assuming the rotor is fixed and the stator rotates in reverse with the same angular speed, the PM field, armature reaction field, and the relative permeance function can be expressed as [12]:

$$B_{mag} = \sum_{n} B_{mn} \cos\left(np\theta\right) \tag{20}$$

$$\begin{aligned} B_{arm} &= \sum_{\nu} B_{av}^{h} \sin\left[\nu N_t \left(\theta + \omega_r t\right) + s_{v,h} \omega_h t\right] \\ &= \sum_{\nu} B_{av}^{h} \sin\left[\nu N_t \theta + \left(\nu N_t \omega_r + s_{v,h} \omega_h\right) t\right] \end{aligned} \tag{21}$$

$$\lambda_a = \lambda_0 + \sum_{u} \lambda_u \cos\left[u Q_s \left(\theta + \omega_r t\right)\right] \tag{22}$$

where, Q_s is stator slot number, ω_r is the rotation angular speed.

According to the Maxwell tensor method, the normal electromagnetic force density acting on the PM surface can be calculated from

$$\begin{aligned} P_z &\approx \frac{1}{2\mu_0}\left[\left(B_{mag} + B_{arm}\right)\lambda_a\right]^2 \\ &= \frac{1}{2\mu_0}\left\{\sum_{n} B_{mn} \cos\left(np\theta\right) + \sum_{\nu} B_{av}^{h} \sin\left[\nu N_t \theta + \left(\nu N_t \omega_r + s_{v,h} \omega_h\right) t\right]\right\}^2 \\ &\times \left\{\lambda_0 + \sum_{\mu} \lambda_\mu \cos\left[u Q_s \left(\theta + \omega_r t\right)\right]\right\}^2. \end{aligned} \tag{23}$$

It is noteworthy that the Maxwell stress is not necessarily a physically conforming distribution. The virtual work method is an alternative method for local force calculation [24]. However, the Maxwell tensor method is still a sufficient approximation to analyze the spatial order and frequency of the electromagnetic force [25].

The armature reaction field generated by the sideband current harmonics caused by rotor position error interacts with the PM field or the armature reaction field itself. Extra sideband electromagnetic force is produced. However, since the amplitude of the sideband current harmonics and the armature reaction field is relatively small, the interaction of the armature reaction field with the fundamental PM field is the dominant source of the electromagnetic force. As a result, the extra force brought by the sideband current harmonics caused by rotor position error can be reduced to:

$$\begin{aligned} &P_{extra} \\ &= \frac{1}{2\mu_0} \lambda_0^2 \sum_{\nu} B_{m1} B_{av}^{h} \begin{Bmatrix} \sin\left[\left(p + \nu N_t\right)\theta + \left(\nu N_t \omega_r + s_{v,h} \omega_h\right) t\right] \\ -\sin\left[\left(p - \nu N_t\right)\theta - \left(\nu N_t \omega_r + s_{v,h} \omega_h\right) t\right] \end{Bmatrix}. \end{aligned} \tag{24}$$

It can be seen from (24) that the rotor position error does not change the spatial order of the electromagnetic force, but only the frequency. Since the electromagnetic force with lower spatial order plays a leading role in the generation of vibration and noise, the influence of position error on zeroth-order and the lowest nonzero N_tth-order force is discussed here.

The zeroth-order electromagnetic force satisfies:

$$p\text{-}\nu N_t = 0. \tag{25}$$

The frequency is written as

$$f_0 = \nu N_t f_r + s_{v,h} f_h = p f_r + s_{v,h} f_h. \tag{26}$$

While the N_tth-order electromagnetic force satisfies:

$$\left|p\text{-}\nu N_t\right| = N_t. \tag{27}$$

The frequency is written as

$$f_{N_t} = \nu N_t f_r + s_{v,h} f_h. \tag{28}$$

Take the fundamental current for example, f_h=f_1=pf_r. The electric motor studied in this paper is with 30 poles and 27slots, p/N_t=3k-1. The zeroth-order electromagnetic force satisfies ν=3k-1 according to (25), and $s_{v,h}$=-1. Therefore, when there is no rotor position error, it can be seen from (26) the frequency of the zeroth-order force is equal to 0. While when the position error is introduced, due to the existence of sideband current harmonics f_1±$P_r f_1$ and f_1±2$P_r f_1$, the frequency of zeroth-order electromagnetic force is as follows:

$$f_0 = \begin{cases} 0 \\ P_r f_1 \\ 2P_r f_1 \end{cases}. \tag{29}$$

The N_tth electromagnetic force satisfies ν=3k+1 according to (27), and $s_{v,h}$=-1 for the fundamental current. Thus, the frequency of the N_tth force generated by the fundamental current is expressed as

$$\begin{aligned} f_{N_t} &= \nu N_t f_r + s_{v,h} f_h \\ &= \left(p - Nt\right) f_r + f_1 \\ &= \left(2p - Nt\right) f_r. \end{aligned} \tag{30}$$

Considering the rotor position error, the frequency of the N_tth force generated is written as

$$f_{N_t}=\begin{cases}(2p-Nt)f_r\\(2p-Nt)f_r\pm P_rf_1=(2p-Nt\pm p_{resolver})f_r\\(2p-Nt)f_r\pm 2P_rf_1=(2p-Nt\pm 2p_{resolver})f_r\end{cases}. \quad (31)$$

In the same way, we can conclude the frequency of the zeroth and N_tth force generated by $(6k\pm1)$th, $(f_s\pm2f_1)$th, and $(f_s\pm4f_1)$th current harmonics, as summarized in Table II.

TABLE II
FREQUENCY OF THE ZEROTH AND N_TTH FORCE WITHOUT POSITION ERROR.

Spatial order	Frequency		
	Fundamental current	$(6k\pm1)$th current harmonics	$(f_s\pm2f_1)$th and $(f_s\pm4f_1)$th current harmonics
0th	0	$6kf_1$	$f_s\pm3f_1$
N_tth	$(2p\text{-}N_t)f_r$	$(6kp\text{-}2p+N_t)f_r$ $(6kp+2p\text{-}N_t)f_r$	$f_s\pm(p+N_t)f_r$ $f_s\pm(5p\text{-}N_t)f_r$

When there exists the position error, extra sideband harmonics with the frequency of $\pm P_rf_1$ and $\pm2P_rf_1$ will be generated around the above electromagnetic force.

E. Effect of Position Error on Electromagnetic Noise

According to [26], the amplitude of vibration displacements of the electric motor can be derived as

$$A_m=\frac{F_m/M}{\sqrt{\left(\omega_m^2-\omega_r^2\right)^2+4\xi_m^2\omega_r^2\omega_m^2}}. \quad (32)$$

The sound power is then calculated from

$$\Pi=\sum_{m,n=0}^{\infty}\sigma_{mn}\rho_0c_0S<\overline{v_{mn}^2}> \quad (33)$$

where F_m is the force, M is the mass of the motor, ω_m is the angular natural frequency, ω_r is the angular frequency of the electromagnetic force, ξ_m is the modal damping ratio, ρ_0 is the sound density, c_0 is the sound speed, σ_{mn} is the sound radiation efficiency, S is the area of radiating surface and v_{mn} is the surface velocity of the motor.

It can be seen from (32) and (33) that the amplitude of the vibration and noise is proportional to that of the electromagnetic force and the frequency is the same as the electromagnetic force. The natural frequency only affects the amplitude of the vibration and noise. Since the rotor position error introduces extra sideband harmonics to the electromagnetic force, sideband harmonics of $\pm P_rf_1$ and $\pm2P_rf_1$ can also be found in the noise spectrum.

The phase current of the healthy motor driven by inverter contains $(6k\pm1)$th current harmonics and high-frequency current harmonics around the switching frequency as well. The effect of low-frequency and high-frequency current harmonics on the acoustic noise has been investigated in our previous studies [11] and [12]. The $(6k\pm1)$th current harmonics will not bring extra frequencies but affect the amplitude of the harmonic noise. However, the inverter brings high-frequency switching noise compared with the electric motors fed by the ideal sinusoidal current.

Besides, the presence of rotor eccentricity usually produces UMP in electric motors. Both the rotor position error and dynamic eccentricity can introduce extra sideband harmonics to the noise spectrum, but their frequency is totally different. According to [27] and [28], static eccentricity will induce additional spatial ±1 and ±2th order electromagnetic force. While dynamic eccentric will change both the spatial order and frequency of the electromagnetic force, resulting in additional spatial orders of ±1 and ±2th and temporal harmonics with the frequency of $\pm f_r$ and $\pm2f_r$. This means static eccentricity will not change the frequency of the noise spectrum, while dynamic eccentricity will introduce extra $\pm f_r$ and $\pm2f_r$ sideband harmonics to the noise spectrum. Since the frequency characteristics of the sideband harmonics differ from those generated by rotor position error, we can distinguish them easily from the tested noise spectrum. This is also a point that deserves our attention in the fault diagnosis of electric motors.

The effect of different origins on the frequency features of noise peaks in electric motors is summarized in Table III. Here, f_{HN} is the frequency of the harmonic noise related to the fundamental and $(6k\pm1)$th current harmonics. f_{SN} is the frequency of the switching noise related to the high-frequency current near the switching frequency. The values of f_{HN} and f_{SN} are the same as those of the electromagnetic forces listed in Table II.

TABLE III
FREQUENCY FEATURES OF THE NOISE PEAKS FROM DIFFERENT ORIGINS

Noise Origins	Harmonic noise	Switching noise
Sine current	f_{HN}	/
Inverter	f_{HN}	f_{SN}
Resolver position error	$f_{HN}\pm P_rf_1$ and $f_{HN}\pm2P_rf_1$	$f_{SN}\pm P_rf_1$ and $f_{SN}\pm2P_rf_1$
Eccentricity	$f_{HN}\pm f_r$ and $f_{HN}\pm2f_r$	$f_{SN}\pm f_r$ and $f_{SN}\pm2f_r$

III. SIMULATION RESULTS

An axial-flux external-rotor in-wheel PMSM with 30 poles and 27 slots is selected to validate the theoretical analysis. The exploded view of the PMSM is shown in Fig. 2a. The in-wheel motor adopts the single-stator-single-rotor topology. The PMs are bonded on the front cover and form the outer rotor system with the shell and end cover. The stator is fixed on the shaft through a stator tray. Fractional slot concentrated winding is adopted, with the advantage of high efficiency, high torque density, and high copper slot fill factor [29]. The position sensor is a variable reluctance resolver with 3 pole pairs, as shown in Fig. 2b. Table IV lists the main parameters of the axial-flux PMSM.

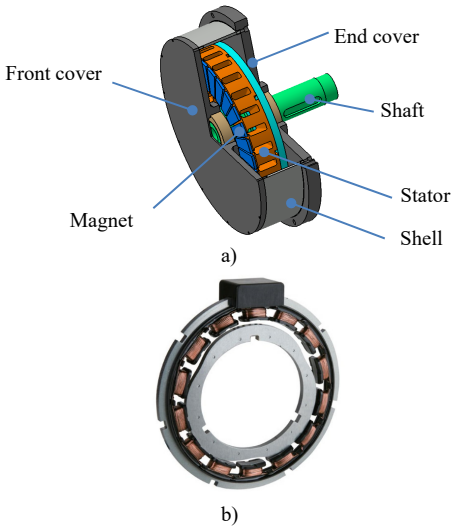

Fig. 2. Structure schematic diagram a) Exploded view of the PMSM [12] b) Resolver

TABLE IV
MAIN PARAMETERS OF PMSM

Description	Value	Description	Value
Pole/Slot number	30/27	Remnant flux density of PM	1.2 T
Pole pair number of resolver	3	d-axis inductance	738 μH
Inner radius of magnet	69 mm	q-axis inductance	738 μH
Outer radius of magnet	112 mm	Stator resistance	0.08 Ω
Length of air-gap	1.5 mm	Rotor flux	0.04 Wb
Slot opening width	3 mm	Switching frequency	10k Hz
Rated speed	600 rpm	DC Bus voltage	200 V
Pole-arc coefficient	0.85	Dead time	2 μs

A. Current

The axial-flux in-wheel motor studied in this paper is a surface-mounted PMSM. When the maximum torque per ampere (MTPA) control strategy is adopted, the reference current of the d-axis is equal to 0, q-axis current is determined by the target torque. PI control is employed by the current regulator, and the output d- and q-axis voltage is converted into the two-phase static coordinate system voltage through the park inverse transformation, and then SVPWM is used to obtain the switching signal. The inverter converts the input DC voltage into three-phase AC current according to the switching signal to drive the motor. In the actual operation of the motor, the three-phase current is obtained by the Hall sensor, and the current signal is input to the current regulator through Clarke and Park transformation, and the position signal is obtained by the resolver. The final established FOC model is shown in Fig.3. The FOC model is implemented in Simulink, a MATLAB-based graphical programming environment for modeling. The detailed description of the FOC model can refer to [30].

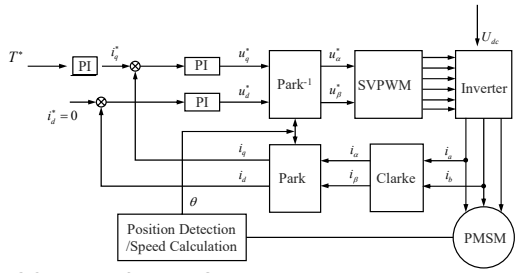

Fig. 3. FOC model of the PMSM

The phase current of the PMSM with and without rotor position error is simulated based on the FOC model. The spectrum is shown in Fig.4 and Fig.5. The rotation speed is 600 rpm and the switching frequency is 10000 Hz. The pole pair number of the PMSM and its resolver is 15 and 3 respectively, thus P_r=0.2. According to Table I, if there is no rotor position error, the frequencies of current harmonics are f_1, $(6k \pm 1)f_1$, and $fs \pm 2kf_1$. The simulation results show that the current harmonics appear at 150, 750, 1050, 9400, 9700, 10300, and 10600 Hz. This is consistent with the previous analysis. When the position error is introduced, extra sideband components can be found near the original current harmonic. According to Table I, the frequency difference of the sideband components is $\pm P_r f_1$ and $\pm 2P_r f_1$. Taking the fundamental current as an example, the simulation results show that when the position error is introduced, additional sideband frequency components are generated at 90, 120, 180, and 210 Hz. While for other current harmonics, the same phenomenon can be found. This suggests that rotor position error produces additional sideband components of ± 30 Hz and ± 60 Hz. The simulation results are consistent with the theoretical analysis results.

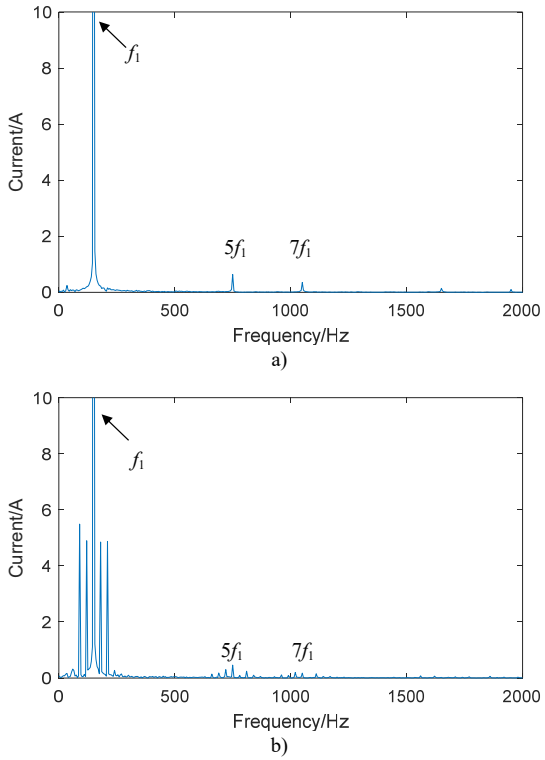

Fig. 4. Spectrum of the low-frequency current at 600 rpm. a) without position error. b) with position error

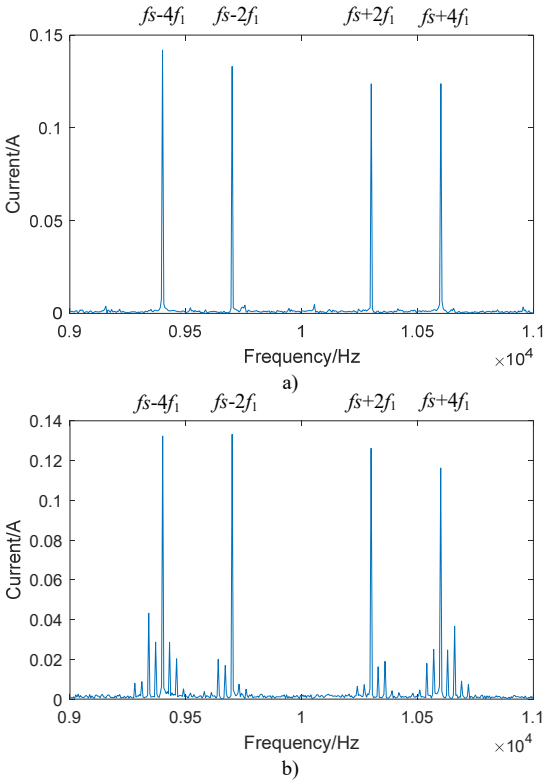

Fig. 5. Spectrum of the high-frequency current at 600 rpm. a) without position error. B) with position error

B. FE modeling

Next, the influence of the rotor position error on electromagnetic force is simulated and analyzed. The electromagnetic FE model of the axial-flux PMSM is established to calculate the air-gap flux density. The general FE modeling process of the PMSM is shown in Fig.6.

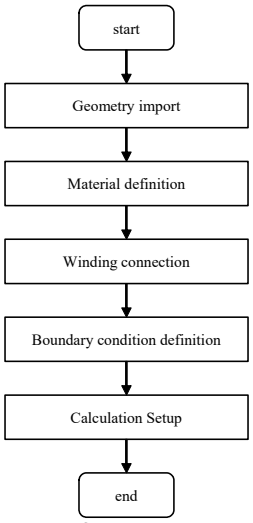

Fig. 6. FE modeling process of the electric motors.

The FE modeling process is briefly described as follows:

1) Geometry import

The structure of axial-flux motors inherently requires the use of a 3-dimensional electromagnetic FE model for accurate analysis. The axial-flux motor studied in this paper has three cycles in space, a 1/3 electromagnetic FE model is built to save the computation time. Meanwhile, the electromagnetic model only needs to contain the effective magnetic circuit, thus active parts including the rotor, stator, PMs, and windings are considered, as shown in Fig.7. The geometry model is input to the FE software firstly.

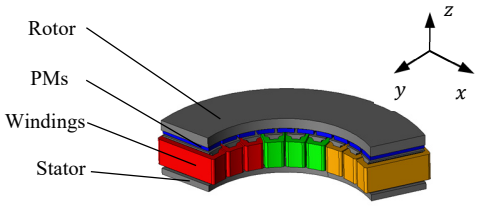

Fig. 7. 1/3 electromagnetic FE model.

2) Material definition

The materials of the rotor, PMs, windings, and stator are then defined, respectively. The material of the PMS is NdFeB. The relative permeability is 1.2 T and the magnetization pattern is along the axial direction. The material of the windings is set to be copper. The material of the stator and rotor is set to be the silicon steel 35JN270 with a lamination coefficient of 0.97.

3) Winding connection

The 30p27s PMSM is a fractional motor with the star connection. The winding connection is shown in Fig.8.The number of turns per coil is set to be 10. The output current of the FOC model serves as the input for the circuit.

4) Boundary condition definition

Since the 1/3 electromagnetic model is adopted, the rotation periodic boundary is needed to restore the real magnetic field

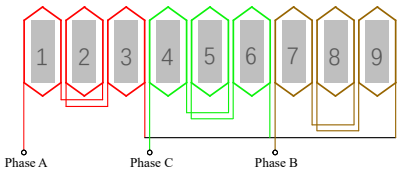

Fig.8 Winding connection of FE model.

distribution. The periodic angle is 120 degrees. Besides, the rotation speed of the rotor is set to be 600 rpm.

5) Calculation setup

The properties of the solver are setup finally. The step time is 2e-5 s and the total calculation steps are 5000. According to the Nyquist sampling theorem, the maximum frequency that can be analyzed is 25000 Hz and the frequency resolution is 10 Hz.

The simulation is performed after all the setup is ready. The air-gap flux density at the average radius can be then extracted from the electromagnetic FE model. The electromagnetic force density is then obtained according to the Maxwell tensor method as shown in (23).

C. Electromagnetic Force

The PMSM rotates with the rated speed 600 rpm during the simulation and the rotating frequency f_r is 10 Hz, thus the frequency of the sideband harmonics caused by rotor position error is ±30 Hz and ±60 Hz theoretically. According to Table II, the spatial order and frequency of the force with and without position error can be concluded, as shown in Table V.

TABLE V
SPATIAL ORDER AND FREQUENCY OF THE ELECTROMAGNETIC FORCE OF THE 30P27S PMSM WITH AND WITHOUT POSITION ERROR

Item	Spatial order	Frequency		
		Fundamental current	$(6k\pm1)$th current harmonics	$(f_s\pm2f_1)$th and $f_s\pm4f_1$)th current harmonics
Without position error	0th	0	$90f_r$	f_s+3f_1
	3rd	$27f_r$	$63f_r$, $117f_r$, $153f_r$,	$f_s\pm18f_r$, $f_s\pm72f_r$
With position error	0th	0 $3f_r$ $6f_r$	$90f_r$,$84f_r$, $87f_r$,$93f_r$,$97f_r$,	$f_s\pm3f_1$, $f_s\pm39f_r$, $f_s\pm42f_r$, $f_s\pm48f_r$, $f_s\pm51f_r$
	3rd	$27f_r$ $21f_r$ $24f_r$ $30f_r$ $33f_r$	①$63f_r$, $57f_r$, $60f_r$, $66f_r$, $69f_r$ ②$117f_r$, $111f_r$, $114f_r$, $120f_r$, $123f_r$ ③$153f_r$, $147f_r$, $150f_r$, $156f_r$, $159f_r$	①$f_s\pm18f_r$, $f_s\pm12f_r$ $f_s\pm15f_r$, $f_s\pm21f_r$, $f_s\pm24f_r$ ②$f_s\pm72f_r$, $f_s\pm66f_r$, $f_s\pm69f_r$, $f_s\pm75f_r$, $f_s\pm78f_r$

There are two requirements to generate the resonance vibration and acoustic noise caused by electromagnetic forces in electric motors. One is that the spatial order of the electromagnetic force should be the same as the circumferential order of the motor mode, and the other is that the frequency of the electromagnetic force is close to its modal frequency. The electromagnetic force is the superposition of a series of rotating force waves with different spatial orders. The electromagnetic force may contain multiple spatial orders for a certain frequency. Therefore, a decomposition of the spatial order and frequency of the electromagnetic force is needed. The two-dimensional fast Fourier transform is performed to analyze the spatial and temporal characteristics of the electromagnetic force, which follows [12]:

$$P_s(r,f)=\int_{-\infty}^{\infty}\int_{-\infty}^{\infty}P_s(\theta,t)e^{-j2\pi(r\theta+ft)}d\theta dt \tag{34}$$

The simulated spatial order and frequency of the electromagnetic force acting on the surface of the magnets with position error are shown in Fig.9. The zeroth-order force with zero frequency has the maximum amplitude among all the electromagnetic forces and its amplitude is 1.9e5 N/m^2. This force only leads to static deformation of the structure and has no influence on the acoustic noise of the electric motors.

Extra sideband components can be observed around the original harmonics. The minimum frequency of zeroth-order force is 900 Hz in ideal condition, and the sideband components appear at 840, 870, 930, and 960 Hz when the rotor position error is introduced. Near the switching frequency, the frequencies of zeroth-order electromagnetic force are 9550 and 10450 Hz, while sideband components also appear at 9550/10450±30 Hz and ±60 Hz when there is position error. The same phenomenon can be observed for the third-order electromagnetic force. The simulation results match well with the theoretical results. This proves the effectiveness of the theoretical analysis in Section II. Since the electromagnetic force is the source of the vibration and noise in electrical motors, the position error will furtherly introduce sideband components to the noise spectrum, making the orders of noise more abundant.

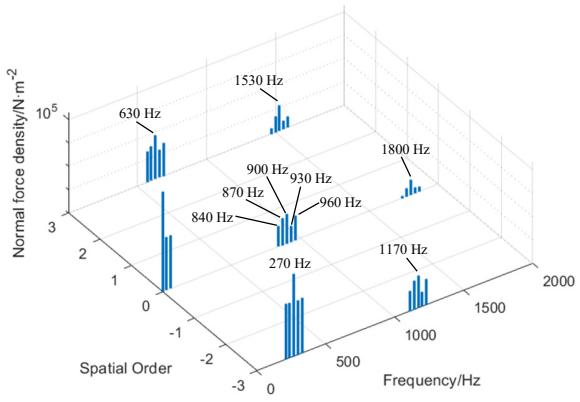

Fig. 9. Spatial order and frequency of the electromagnetic force with rotor position error. a) Low-frequency force. b) High-frequency force near the switching frequency.

IV. Experiment Results and Analysis

The noise of the PMSM is measured in a semi-anechoic room to validate the above theoretical analysis furtherly. The motor is mounted on a quarter-car suspension bench, as shown in Fig.10. Four microphones are used to capture the radiation noise. Since the PMs are connected with the front cover directly, microphone 4 has the largest noise level among all microphones. The three-phase current is recorded by the current clamp.

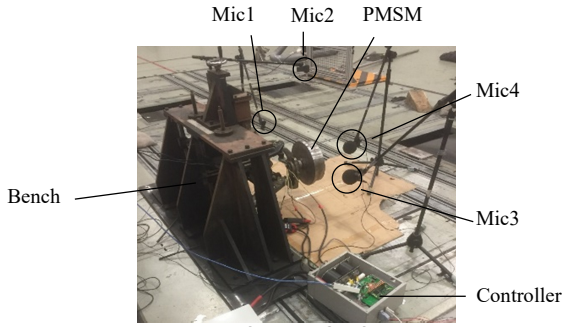

Fig. 10. Experimental setup of the PMSM for noise test

Fig.11 shows the current waterfall plot during acceleration. 0.6th, 0.8th, 1.2th, and 1.4th current harmonics can be found around the fundamental current in Fig.11a. While for the high-frequency current harmonics near the switching frequency, additional $\pm 0.2f_1$ and $\pm 0.4f_1$ sideband components are also induced near the original current harmonics $f_s \pm 2f_1$ and $f_s \pm 4f_1$, as shown in Fig.11b. The experiment results match well with the analytical and simulation results.

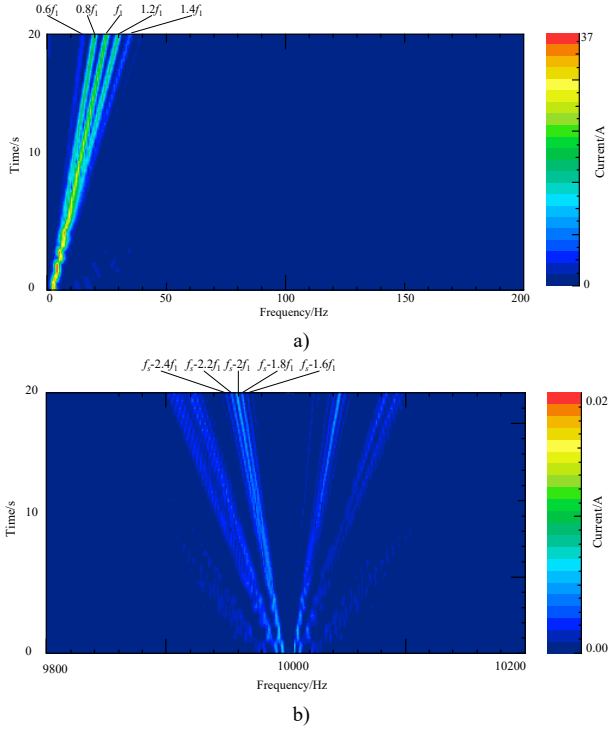

Fig. 11. Time-frequency map of the tested phase current. a) Low-frequency current harmonics b) High-frequency current harmonics

The tested sound pressure level (SPL) at rated speed 600 rpm is shown in Fig.12. The test is performed under no load condition with the PMSM idling to eliminate the influence of tire noise. The amplitude of current is not zero as the motor has

to overcome the rotating damping. Actually, the load only affects the amplitude of the current, but has no effect on its frequency characteristics. Rotor position error brings sideband harmonics to the current spectrum both in no load and heavy load condition. As a result, the effect of rotor position error on the frequency feature of the noise spectrum under different load conditions can be expected to be the same as well.

The modal shapes and frequencies of the 0th and 3rd modes are shown in Fig.13. The natural frequency has a significant effect on the amplitude of the vibration and noise. Different from traditional radial-flux motors, the zeroth-order electromagnetic force is the main source of the vibration and noise for axial-flux motors as the modal frequency of zeroth mode is the lowest. For the zeroth-order force, the frequency is $6kpf_r$ when there is no position error. From Fig.12, we can see the maximum peak noise appears at 900 Hz, which is mainly caused by the zeroth-order force. Rotor position error will bring extra sideband harmonics to the current with the frequency of $f_h \pm 0.4f_1$ and $f_h \pm 0.2f_1$. The armature reaction field generated by these sideband harmonics interacts with the PM field and produces extra electromagnetic force near 900 Hz. According to Table III, the frequency of zeroth-order force is 840, 870, 930, and 960 Hz with rotor position error. Consequently, noise peaks appear at these frequencies as well, as shown in Fig. 12a. The amplitude of these noise peaks around 900Hz is given in Table VI. It can be seen from Table VI that the amplitude of these sideband harmonics at 840, 870, 930, and 960 Hz is considerable compared with that of the original one at 900 Hz. Hence, the effect of rotor position error on the vibration and noise cannot be neglected. According to Table II, the frequency of the 3rd spatial order axial force is 270, 630, and 1170 Hz, etc. The 3rd spatial order axial force also causes noise peaks at these frequencies. but the amplitude is relatively small due to the high frequency of the 3rd mode. Besides, a remarkable resonance can be observed near 700 Hz. This is mainly due to the existence of the 0th natural mode at this frequency.

As shown in Fig.12b, the amplitude of the high-frequency switching noise due to inverter modulation is small compared with that in Fig.12a. This means the contribution of the switching noise to the over SPL is small, but it has a significant influence on the sound quality of electric motors [31]. The switching noise will worsen the tonality, sharpness, sensitivity, and subjective scores. It cannot be ignored in the analysis of the acoustic noise of electric motors. The frequency of zeroth-order force is $f_s \pm 3f_1$ without position error. It can be seen from Fig.12b, noise peaks appear at 9550 and 10450 Hz. Many sideband harmonics can also be found in Fig.12b at 9550±30, 9550±60, 10450±30, and 10450±60 Hz due to the potion error. Meanwhile, noise peaks also appear at 9820 and 10180 Hz, which are caused by the 3rd-order force. Due to the additional current harmonics caused by position error, the electromagnetic force produces extra ± 30 and ± 60 Hz sideband components near 9820 and 10180 Hz, which are also reflected in the noise spectrum. The experimental results are consistent with the theoretical results. This validates the above analysis about the influence of rotor position error on electromagnetic noise.

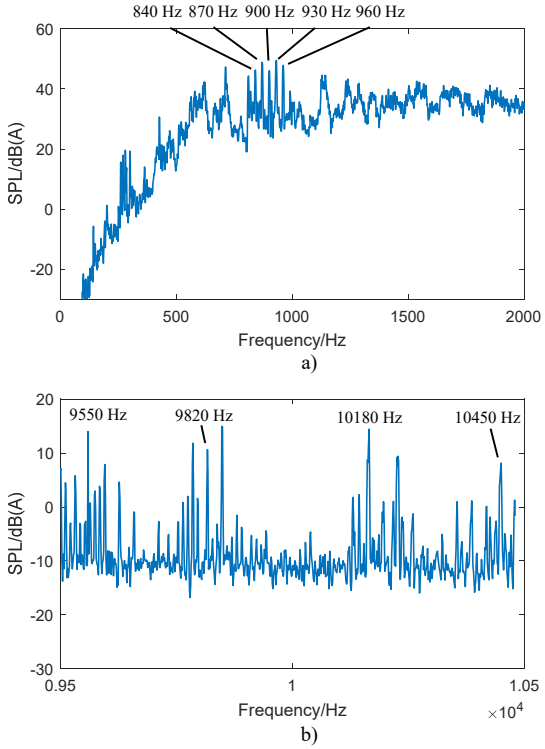

Fig. 12. Tested noise spectrum at 600 rpm. a) Low-frequency noise b) high-frequency noise near the switching frequency

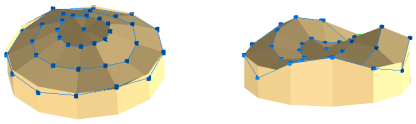

a) b)

Fig. 13. Modal shapes of the PMSM. a)0th: 665 Hz b)3rd: 4400 Hz.

TABLE VI
AMPLITUDE OF SOUND PRESSURE LEVEL

Frequency/Hz	SPL/dB(A)
900	46.3
840	48.8
870	46
930	49.5
960	47.8

V. CONCLUSIONS

The influence of rotor position error on the electromagnetic noise of PMSM is investigated in this paper. The main conclusions are as follows,

1) The rotor position error caused by amplitude imbalance and imperfect quadrature of the resolver will bring $\pm 2P_rf_1$ sideband harmonic in the stator phase current, and that caused by dc offset will bring $\pm P_rf_1$ sideband current harmonic.

2) The rotor position error will not change the spatial order of the electromagnetic force, but introduce extra $\pm P_{resloverf_r}$ and $\pm 2P_{resloverf_r}$ sideband components. This leads to extra sideband harmonics in the noise spectrum.

This paper establishes a generic theoretical formulation, which is independent of the details of motor geometry. Although an axial flux PMSM is selected to validate the theoretical analysis. the conclusions of this paper are also

applicable to the radial flux PMSM. This study benefits the fault diagnosis and noise source identification of electric motors. The next step is to investigate the compensation method of rotor position error to suppress these sideband harmonics for electric motors in vehicle applications.

APPENDIX

A phase current can be calculated from

$$
\begin{aligned}
i_a &\approx i_q\theta_{err}\cos\theta_e - i_q\sin\theta_e \\
&= \begin{Bmatrix} I_{q1} + I_{q\_6k}\left[\cos\left(6k\omega_1 t+\varphi_q\right)\right] \\ +I_{q\_\omega_s\pm 3\omega_1}\left[\cos\left(\omega_s t\pm 3\omega_1 t+\varphi_q\right)\right]\end{Bmatrix}\bullet\begin{Bmatrix}\begin{bmatrix}\frac{\alpha}{2}\sin\left(2P_r\theta_e\right)-\frac{\beta}{2}\left(1+\cos 2P_r\theta_e\right) \\ -\frac{U_{offset}}{KE}\cos P_r\theta_e\end{bmatrix}\cos\theta_e - \sin\theta_e\end{Bmatrix} \\
&= \begin{Bmatrix} I_{q1} + I_{q\_6k}\left[\cos\left(6k\omega_1 t+\varphi_q\right)\right] \\ +I_{q\_\omega_s\pm 3\omega_1}\left[\cos\left(\omega_s t\pm 3\omega_1 t+\varphi_q\right)\right]\end{Bmatrix}\bullet\begin{Bmatrix}\frac{\alpha}{4}\left[\sin\left(1+2P_r\right)\theta_e-\sin\left(1-2P_r\right)\theta_e\right] \\ -\frac{\beta}{4}\left[\cos\left(1+2P_r\right)\theta_e+\cos\left(1-2P_r\right)\theta_e\right]-\frac{\beta}{2}\cos\theta_e \\ -\frac{U_{offset}}{2KE}\left[\cos\left(1+P_r\right)\theta_e+\cos\left(1-P_r\right)\theta_e\right] \\ -\sin\theta_e\end{Bmatrix} \\
&= -\begin{Bmatrix} I_{q1} + I_{q\_6k}\left[\cos\left(6k\omega_1 t+\varphi_q\right)\right] \\ +I_{q\_\omega_s\pm 3\omega_1}\left[\cos\left(\omega_s t\pm 3\omega_1 t+\varphi_q\right)\right]\end{Bmatrix}\sin\theta_e \\
&\quad + \begin{Bmatrix} I_{q1} + I_{q\_6k}\left[\cos\left(6k\omega_1 t+\varphi_q\right)\right] \\ +I_{q\_\omega_s\pm 3\omega_1}\left[\cos\left(\omega_s t\pm 3\omega_1 t+\varphi_q\right)\right]\end{Bmatrix}\begin{Bmatrix}\frac{\alpha}{4}\left[\sin\left(1+2P_r\right)\theta_e-\sin\left(1-2P_r\right)\theta_e\right] \\ -\frac{\beta}{4}\left[\cos\left(1+2P_r\right)\theta_e+\cos\left(1-2P_r\right)\theta_e\right]-\frac{\beta}{2}\cos\theta_e \\ -\frac{U_{offset}}{2KE}\left[\cos\left(1+P_r\right)\theta_e+\cos\left(1-P_r\right)\theta_e\right]\end{Bmatrix}.
\end{aligned}
\tag{35}
$$

REFERENCES

[1] W. Deng and S. Zuo, "Electromagnetic Vibration and Noise of the Permanent-Magnet Synchronous Motors for Electric Vehicles: An Overview," IEEE Trans. Transport. Electrific., vol. 5, no. 1, pp. 59-70, 2019, doi: 10.1109/tte.2018.2875481.

[2] P. Sunghyuk, K. Wonho, and K. Sung-Il, "A Numerical Prediction Model for Vibration and Noise of Axial Flux Motors," IEEE Trans. Ind. Electron., vol. 61, no. 10, pp. 5757-5762, Oct 2014, doi: 10.1109/tie.2014.2300034.

[3] F. Lin, S. G. Zuo, W. Z. Deng, and S. L. Wu, "Modeling and Analysis of Acoustic Noise in External Rotor In-Wheel Motor Considering Doppler Effect," IEEE Trans. Ind. Electron., vol. 65, no. 6, pp. 4524-4533, Jun 2018, doi: 10.1109/Tie.2017.2758742.

[4] J. L. Besnerais et al., "Multiphysics Modeling: Electro-Vibro-Acoustics and Heat Transfer of PWM-Fed Induction Machines," IEEE Trans. Ind. Electron., vol. 57, no. 4, pp. 1279-1287, 2010, doi: 10.1109/TIE.2009.2029526.

[5] S. Wu, W. Tong, W. Li, S. Yu, and R. Tang, "Electromagnetic Vibration Analysis of High-Speed Permanent Magnet Synchronous Machines With Amorphous Metal Stator Cores Considering Current Harmonics," IEEE Trans. Ind. Electron., vol. 67, no. 12, pp. 10156-10167, 2020, doi: 10.1109/tie.2019.2959501.

[6] S. Wang, J. Hong, Y. Sun, and H. Cao, "Analysis of Zeroth-Mode Slot Frequency Vibration of Integer Slot Permanent-Magnet Synchronous Motors," IEEE Trans. Ind. Electron., vol. 67, no. 4, pp. 2954-2964, 2020.

[7] H. Fang, D. Li, R. Qu, and P. Yan, "Modulation Effect of Slotted Structure on Vibration Response in Electrical Machines," IEEE Trans. Ind. Electron., vol. 66, no. 4, pp. 2998-3007, 2019, doi: 10.1109/tie.2018.2847639.

[8] S. Wang, J. Hong, Y. Sun, and H. Cao, "Effect Comparison of Zigzag Skew PM Pole and Straight Skew Slot for Vibration Mitigation of PM Brush DC Motors," IEEE Trans. Ind. Electron., vol. 67, no. 6, pp. 4752-4761, 2020, doi: 10.1109/tie.2019.2927175.

[9] Y.-H. Jung, M.-R. Park, and M.-S. Lim, "Asymmetric Rotor Design of IPMSM for Vibration Reduction Under Certain Load Condition," IEEE Trans. Energy Convers., vol. 35, no. 2, pp. 928-937, 2020.

[10] K. Wang, Z. Gu, Z. Q. Zhu, and Z. Z. Wu, "Optimum Injected Harmonics into Magnet Shape in Multi-Phase Surface-Mounted PM Machine for Maximum Output Torque," IEEE Trans. Ind. Electron., vol. PP, no. 99, pp. 1-1, 2017, doi: 10.1109/TIE.2017.2669888.

[11] F. Lin, S. G. Zuo, W. Z. Deng, and S. L. Wu, "Modeling and Analysis of Electromagnetic Force, Vibration, and Noise in Permanent-Magnet Synchronous Motor Considering Current Harmonics," IEEE Trans. Ind. Electron., vol. 63, no. 12, pp. 7455-7466, Dec 2016, doi: 10.1109/Tie.2016.2593683.

[12] W. Deng and S. Zuo, "Comparative Study of Sideband Electromagnetic Force in Internal and External Rotor PMSMs With SVPWM Technique," IEEE Trans. Ind. Electron., vol. 66, no. 2, pp. 956-966, 2019, doi: 10.1109/tie.2018.2821110.

[13] Y. Fang and T. Zhang, "Vibroacoustic Characterization of a Permanent Magnet Synchronous Motor Powertrain for Electric Vehicles," IEEE Trans. Energy Convers., vol. PP, no. 99, pp. 1-1, 2017, doi: 10.1109/TEC.2017.2737483.

[14] S. G. Zuo, F. Lin, and X. D. Wu, "Noise Analysis, Calculation, and Reduction of External Rotor Permanent-Magnet Synchronous Motor," IEEE Trans. Ind. Electron., vol. 62, no. 10, pp. 6204-6212, Oct 2015, doi: 10.1109/Tie.2015.2426135.

[15] W. Lee, J. J. Moon, W. S. Im, J. H. Park, and J. M. Kim, "Classification and Compensation of DC Offset Error and Scale Error in Resolver Signals," Journal of Power Electronics, vol. 16, no. 3, pp. 1190-1199, 2016.

[16] R. Alipour-Sarabi, Z. Nasiri-Gheidari, F. Tootoonchian, and H. Oraee, "Effects of Physical Parameters on the Accuracy of Axial Flux Resolvers," IEEE Trans. Magn., vol. 53, no. 4, pp. 1-11, 2017.

[17] J. Lara, J. Xu, and A. Chandra, "Effects of Rotor Position Error in the Performance of Field-Oriented-Controlled PMSM Drives for Electric Vehicle Traction Applications," IEEE Trans. Ind. Electron., vol. 63, no. 8, pp. 4738-4751, 2016.

[18] W. Z. Deng and S. G. Zuo, "Axial Force and Vibroacoustic Analysis of External-Rotor Axial-Flux Motors," IEEE Trans. Ind. Electron., vol. 65, no. 3, pp. 2018-2030, Mar 2018, doi: 10.1109/Tie.2017.2739697.

[19] Y. Mao, S. Zuo, and J. Cao, "Effects of Rotor Position Error on Longitudinal Vibration of Electric Wheel System in In-Wheel PMSM Driven Vehicle," IEEE/ASME Transactions on Mechatronics, vol. 23, no. 3, pp. 1314-1325, 2018, doi: 10.1109/tmech.2018.2818260.

[20] S. H. Hwang, H. J. Kim, J. M. Kim, L. Liu, and H. Li, "Compensation of Amplitude Imbalance and Imperfect Quadrature in Resolver Signals for PMSM Drives," IEEE Trans. Ind. Appl., vol. 47, no. 1, pp. 134-143, 2011.

[21] Z. Tang and B. Akin, "A New LMS Algorithm Based Deadtime Compensation Method for PMSM FOC Drives," IEEE Trans. Ind. Appl., vol. 54, no. 6, pp. 6472-6484, 2018, doi: 10.1109/TIA.2018.2853045.

[22] W. Liang, J. Wang, P. C. K. Luk, W. Fang, and W. Fei, "Analytical Modeling of Current Harmonic Components in PMSM Drive With Voltage-Source Inverter by SVPWM Technique," IEEE Trans. Energy Convers., vol. 29, no. 3, pp. 673-680, 2014, doi: 10.1109/TEC.2014.2317072.

[23] Y. J. Zhang, S. L. Ho, H. C. Wong, and G. D. Xie, "Analytical prediction of armature-reaction field in disc-type permanent magnet generators," IEEE Trans. Energy Convers., vol. 14, no. 4, pp. 1385-1390, Dec 1999, doi: Doi 10.1109/60.815077.

[24] L. H. De Medeiros and G. J. I. T. o. M. Reyne, "About the distribution of forces in permanent magnets," vol. 35, no. 3, pp. 1215-1218, 1999.

[25] J. Krotsch and B. Piepenbreier, "Radial Forces in External Rotor Permanent Magnet Synchronous Motors With Non-Overlapping Windings,", IEEE Trans. Ind. Electron., vol. 59, no. 5, pp. 2267-2276, May 2012, doi: 10.1109/Tie.2011.2151827.

[26] J. F. Gieras, C. Wang, and J. C. Lai, Noise of polyphase electric motors. CRC/Taylor & Francis, 2006.

[27] F. Lin, S. G. Zuo, and W. Z. Deng, "Impact of rotor eccentricity on electromagnetic vibration and noise of permanent magnet synchronous motor," Journal of Vibroengineering, vol. 20, no. 2, pp. 923-935, Mar 2018, doi: 10.21595/jve.2017.18436.

[28] S. Abdi, E. Abdi, H. Toshani, and R. McMahon, "Vibration Analysis of Brushless Doubly Fed Machines in the Presence of Rotor Eccentricity," IEEE Trans. Energy Convers., vol. 35, no. 3, pp. 1372-1380, 2020, doi: 10.1109/TEC.2020.2987100.

[29] A. El-Refaie, "Fractional-Slot Concentrated-Windings Synchronous Permanent Magnet Machines: Opportunities and Challenges," IEEE Trans. Ind. Electron., vol. 57, no. 1, pp. 107-121, 2010, doi: 10.1109/TIE.2009.2030211.

[30] J. Pyrhonen, V. Hrabovcova, and R. S. Semken, Electrical machine drives control: An introduction. John Wiley & Sons, 2016.

[31] Y. Fang and T. Zhang, "Sound Quality of the Acoustic Noise Radiated by PWM-Fed Electric Powertrain," (in English), IEEE Trans. Ind. Electron., vol. 65, no. 6, pp. 4534-4541, Jun 2018, doi: 10.1109/Tie.2017.2767558.

Wenzhe Deng was born in Xuzhou city, Jiangsu, China, in 1993. He received the B.S.E. degree in automotive engineering, Jilin University, Changchun, Jilin, China, in 2014 and the PhD degree in 2019 in automotive engineering, Tongji University, Shanghai, China. He is currently an associate professor of School of Electrical Engineering and Automation, Anhui University, Hefei, China.

His research interests include vibration and noise of PMSM and axial flux motors, vehicle vibration and noise control.

Shuguang Zuo was born in Yuanjiang city, Hunan, China, in 1968. He received the B.S.E. degree in mechanical design, Hunan Agricultural University, Changsha, Hunan, China, in 1990. He received the M.S. degree in 1993 and the PhD degree in 1996 in automotive engineering, Jilin University, Changchun, Jilin, China.

From 1996 to 1998, He was a Postdoctoral Researcher with Aviation and Aerospace Technology Postdoctoral Research Station, Nanjing Aeronautics and Astronautics University, Nanjing, Jiangsu, China. He is currently Professor of College of Automotive Engineering, Tongji University, Shanghai, China. His research interests include vehicle system dynamics and control, vehicle vibration and noise control, and vibration and noise of electrical machines.